ARTICLE NO. 79-0792R

G80-060

# Active Controls for Flutter Suppression and Gust Alleviation in Supersonic Aircraft

00016
80001
80004

E. Nissim* and I. Lottati†
*Technion—Israel Institute of Technology, Haifa, Israel*

**Application is made in the present paper of the recently developed relaxed aerodynamic energy concept and synthesis techniques to the definition of appropriate active control systems for the low-speed flutter model of the B-2707-300 supersonic cruise airplane. The effectiveness of the resulting activated systems is analytically tested for flutter suppression, wing root bending moment alleviation, and ride control (fuselage accelerations). The results obtained indicate that considerable increase in flutter speeds can be obtained by the various control systems, using a single trailing-edge control. In all cases, the flutter suppression control system led to a substantial reduction in both wing root bending moments and in fuselage and wing accelerations.**

## Introduction

THEORETICAL analyses and wind tunnel tests of a low-speed flutter model (1/20 scale) of the B-2707-300 airplane (Fig. 1), were conducted under the supersonic transport (SST) Follow-on Program—Phase II.[1] Reference 1 states that "two constraints of the airplane made a flutter-free design unusually difficult: 1) the relatively low payload/total weight ratio made additional structural weight or mass balance particularly distasteful, and 2) any arrangement of lifting surface planforms, thickness, or major mass relocation (e.g., nacelles) degraded the delicate cruise economy or c.g. balance." Because of this flutter dilemma, considerable efforts were directed towards the development of an active flutter suppression system with the objective of improving the flutter speeds of the SST airplane.

Reference 1 shows that the developed flutter suppression system yields only minor improvements in flutter speeds (9.4% increase with activated inboard ailerons, 3.2% increase with activated outboard ailerons, and 11.3% increase with activated inboard and outboard ailerons). The purpose of the present work is to apply the recently developed relaxed energy concept[2] and synthesis techniques[3] to the definition of an appropriate active control system for flutter suppression. The effectiveness of the resulting activated system is then analytically tested for flutter suppression, root bending moment alleviation, and ride control (fuselage and wing accelerations).

Previous analytical applications of the relaxed energy concept for flutter suppression involved the BQM-34E/F drone aircraft[3,4] (with a research supercritical wing) and the YF-17 fighter aircraft[5] (suppression of three different configurations of wing store flutter). The present work supplements the applications to include supersonic type cruise aircraft and is also the first one to investigate the effectiveness of the flutter suppression system (as obtained through the use of the relaxed energy concept), not only for flutter suppression but also for gust alleviation and ride control.

## Description of SST Model and Mathematical Representation

### Description of the SST Model

Figure 1 shows the general layout of the B-2707-300 low-speed flutter model. As can be seen it is possible to activate the two trailing-edge (t.e.) ailerons and the horizontal stabilizer. In Ref. 1, activation of the two ailerons was attempted for purpose of flutter suppression and activation of the horizontal stabilizer (with geared elevator) was attempted for purpose of rigid-body stability augmentation. In the present work, activation of the outboard aileron only will be attempted. This follows the results of a previous investigation[6] which showed that for flutter suppression, the activated system should be located as near the tip of the wing as possible. The outboard aileron measures 13.4% of the wing semi-span and 26% of the wing chord. Its mid-span line is located around 72% of the wing semi-span.

### Equations of Motion and Their Solution

The equations of motion are formulated and solved (for both flutter suppression and gust alleviation problems) following identical lines as outlined in Refs. 3-5, 7. The flutter results are presented by root locus type plots taking the dynamic pressure $Q_D$ as a parameter. The gust alleviation and ride control results are obtained from a continuous gust program, using unit rms gust input based on a Von Kármán gust spectrum.

### Control Law

The general form of the control law employed in this work was established in Ref. 2 using the relaxed energy approach.

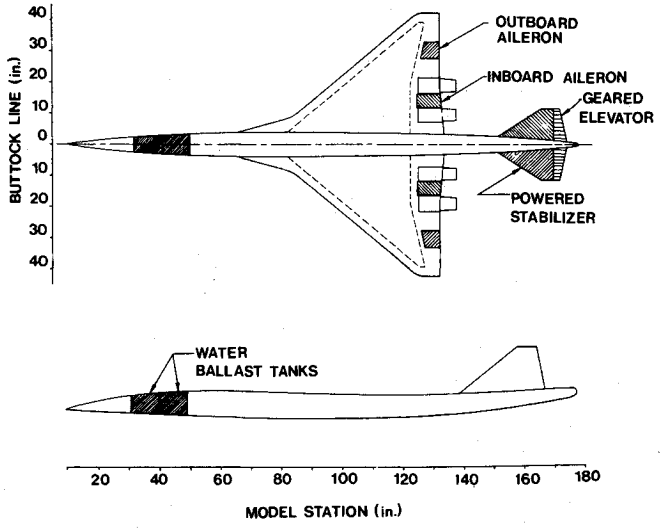


Presented as Paper 79-0792 at the AIAA/ASME 20th Structures and Structural Dynamics Conference, St. Louis, Mo., April 4-6, 1979; submitted April 26, 1979; revision received Sept. 5, 1979. 

Index categories: Guidance and Control; Structural Design; Aeroelasticity and Hydroelasticity.

*Professor, Dept. of Aeronautical Engineering. Member AIAA.

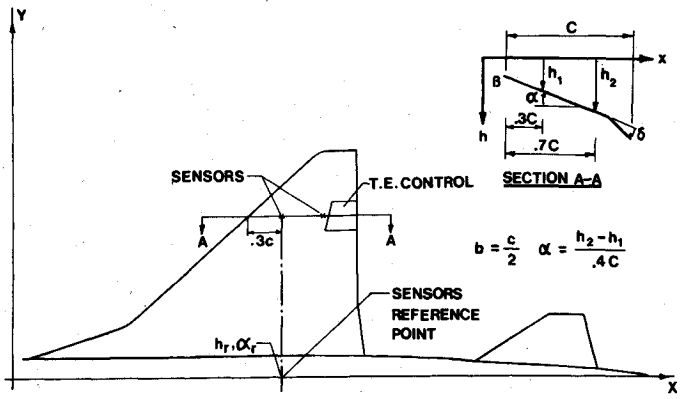


**Fig. 2 Geometrical description of the active control system.**

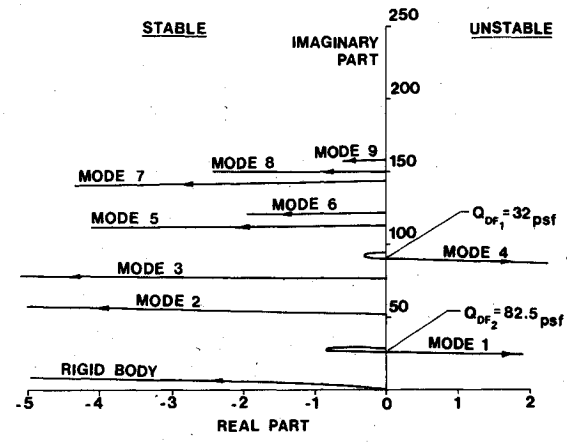


**Fig. 3 Open-loop root locus plot at $M=0.2$.**

The control law for the t.e. control surface is given by the following general form:

$$\delta = -1.86(\alpha_1 - \alpha_r) + R_T \lfloor 4 \quad 2.8 \rfloor \begin{Bmatrix} \dfrac{h_1 - h_r}{b} \\ \alpha_1 - \alpha_r \end{Bmatrix} \tag{1}$$

where $\delta$ is the deflection of the t.e. control surface (see Fig. 2) and where $h_1$, $\alpha_1$ denote the translation and rotation of the 30% chord point of the control surface mid-span section, respectively (see Fig. 2). The parameters $h_r$ and $\alpha_r$ similarly denote the translation and rotation of a reference point located along the center line of the fuselage and $b$ denotes the semi-chord length at the control surface mid-span section (see Fig. 5). $R_T$ is defined by the following expression (see also Refs. 2, 3):

$$R_T = \frac{a_1 S^2}{S^2 + 2\zeta_1 \omega_{n_1} S + \omega_{n_1}^2} + \frac{a_2 S^2}{S^2 + 2\zeta_2 \omega_{n_2} S + \omega_{n_2}^2} \tag{2}$$

The parameters $\alpha_i$, $\zeta_i$, $\omega_{n_i}$ are all positive and their values determined by an optimization program based on the gust response of the aircraft under consideration following the method of Ref. 3.

#### Mathematical Model

The equations of motion, included two rigid-body modes (plunge and pitch) and nine symmetric elastic modes. The generalized aerodynamic forces were computed using the Doublet-Lattice method. The generalized inertia and elastic matrices for the flutter model were supplied by the aircraft manufacturing company together with the mode shapes. The t.e. control was assumed to be mass balanced.

## Objectives

The following objectives were set for the present work:

1) To define control systems for different values of assumed maximum flight dynamic pressure (with $M=0.2$) to determine whether an upper bound exists for flutter speed (while activating a single t.e. control).

2) To check the effectiveness of the resulting flutter suppression systems in reducing the wing root bending moments (b.m.) and in reducing the accelerations of the aircraft due to continuous gust inputs.

3) To spot check the effectiveness for flutter suppression of a control system, as defined in objective 1, above, at a higher Mach number, such as $M=0.9$.

## Presentation and Discussion of Results

The presentation and discussion of results will be grouped under three major headings involving flutter suppression, gust alleviation and ride control characteristics.

#### Flutter Suppression Systems

The effectiveness of the activated t.e. control system can only be assessed by comparison with the open-loop system. The open-loop root locus plots for $M=0.2$ and $M=0.9$ are presented in Figs. 3 and 4. It can be seen that for $M=0.2$, two flutter dynamic pressures ($Q_{DF}$) exist: the first with $Q_{DF}=32$ psf (for zero structural damping $g$) and $\omega_F=89.7$ rad/s, and the second with $Q_{DF}=82.5$ psf (for $g=0$) and $\omega_F=25.1$ rad/s. Similarly, for $M=0.9$, three flutter speeds exist with the following values (for $g=0$): $Q_{DF}=33$ psf with $\omega_F=81.8$ rad/s, $Q_{DF}=74.5$ psf with $\omega_F=21.8$ rad/s, and $Q_{DF}=78.5$ psf with $\omega_F=68.7$ rad/s. Since some of the above flutter branches represent mild flutter instabilities the values of $Q_{DF}$ for the cases where $g=0.015$ and $g=0.03$ are included in a summarizing table (Table 1). It is interesting to note that the lowest value of $Q_{DF}$ increases from $Q_{DF}=32$ psf at $M=0.2$ and $g=0$ to $Q_{DF}=51$ psf at $M=0.2$ and $g=0.03$. For $M=0.9$ the corresponding values of $Q_{DF}$ vary from $Q_{DF}=33$ psf when $g=0$ to $Q_{DF}=37$ psf when $g=0.03$, thus indicating the existence of a more violent flutter.

#### *Determination of the Control Law Parameters*

The control law parameters are determined through the use of an optimization program which minimizes the root mean square rms deflection rates of the control surface due to a unit rms gust input based on the Von Kármán gust spectrum. This procedure is described in detail in Ref. 3.

The optimization was performed at two different flight dynamic pressures: at $Q_D=75$ psf and at $Q_D=89$ psf, while maintaining $M=0.2$. The optimization procedure yields the following optimal control laws:

For $Q_D=75$ psf

$$\delta = \left[ \lfloor 0 \quad -1.86 \rfloor + \left( \frac{0.5S^2}{S^2 + 2\times 1 \times 34.4S + (34.4)^2} + \frac{3.33S^2}{S^2 + 2\times 0.5 \times 100.6S + (100.6)^2} \right) \lfloor 4 \quad 2.8 \rfloor \right] \cdot \begin{Bmatrix} \dfrac{h_1 - h_r}{b} \\ \alpha_1 - \alpha_r \end{Bmatrix} \tag{3}$$

with

$\dot{\delta}_{\text{rms}} = 14.37$ deg/s/ft/s

$\delta_{\text{rms}} = 0.236$ deg/ft/s

**Table 1 Summary of flutter results**

| | Open-loop | | Closed-loop control law I | | Closed-loop control law II |
|---|---|---|---|---|---|
| | $M=0.2$ | $M=0.9$ | $M=0.2$ | $M=0.9$ | $M=0.2$ |
| Flutter $Q_D$, psf | | | | | |
| $g=0$ | 32 | 33 | 84 (163%)[a] | 76 (130%)[a] | 89 (178%)[a] |
| $g=0.015$ | 42 | 35 | 88 (110%)[a] | 77 (120%)[a] | 91 (117%)[a] |
| $g=0.03$ | 51 | 37 | 91 ( 78%)[a] | 78 (110%)[a] | 94 ( 84%)[a] |
| Max. value[b] of $\dot{\delta}_{rms}$, deg/s/fT/s | | | | | |
| $g=0$ | ... | ... | 14.37 | 10.90 | 23.81 |
| $g=0.015$ | ... | ... | 11.89 | 10.54 | 18.72 |
| $g=0.03$ | | ... | 10.92 | 10.24 | 16.17 |
| Max. value[b] of $\delta_{rms}$, deg/ft/s | ... | | | | |
| $g=0$ | ... | ... | 0.236 | 0.262 | 0.789 |
| $g=0.015$ | ... | ... | 0.200 | 0.248 | 0.609 |
| $g=0.03$ | ... | ... | 0.186 | 0.238 | 0.515 |

[a] % Increase in $Q_D$ due to activation of the outboard t.e. control.
[b] Up to dynamic pressure of $Q_D$ optimization.

For $Q_D=89$ psf

$$\delta=\left[\lfloor 0 \quad -1.86\rfloor+\left(\frac{0.8S^2}{S^2+2\times0.5\times20S+(20)^2}+\frac{7.62S^2}{S^2+2\times0.5\times100S+(100)^2}\right)\lfloor 4 \quad 2.8\rfloor\right]\cdot\begin{Bmatrix}\dfrac{h_l-h_r}{b}\\ \alpha_l-\alpha_r\end{Bmatrix} \tag{4}$$

with

$\dot{\delta}_{rms}=23.81$ deg/s/ft/s

$\delta_{rms}=0.789$ deg/ft/s

The control law given by Eq. (3) will be referred to as control law I, whereas the one given by Eq. (4) will be referred to as control law II. The meaning of the different parameters of the control laws, Eqs. (3) and (4), is explained in Refs. 2 and 3. There is no intention to repeat the various details herein except for the statement that the above results show that for minimum control rates, maximum damping is introduced around the frequency of 100 rad/s whereas the minimum flutter frequency is around 90 rad/s. A secondary damping concentration is introduced by the above control laws at frequencies which vary with the optimization $Q_D$. For $Q_D=75$ psf the frequency is around 34 rad/s whereas for $Q_D=89$ psf the frequency is around 20 rad/s. Both frequencies relating to the secondary damping concentration are in the neighborhood of the frequency relating to the second open-loop flutter branch located around 25 rad/s.

*Closed-Loop Performance*

The effectiveness of the above control laws in flutter suppression at $M=0.2$ is shown in Figs. 5 and 6. As can be seen, the flutter branch relating to $Q_{DF}=32$ psf and $\omega=89.7$ rad/s (for the open-loop case) is suppressed and yields no flutter up to the maximum dynamic pressure used for the root locus plots (that is up to $Q_D=120$ psf). On the other hand, the flutter branch associated with the open-loop values of $Q_{DF}=82.5$ psf and $\omega=25.1$ rad/s is only slightly affected by the activated t.e. system. For control law I, the value of $Q_{DF}$ associated with this branch is increased to $Q_{DF}=84$ psf and

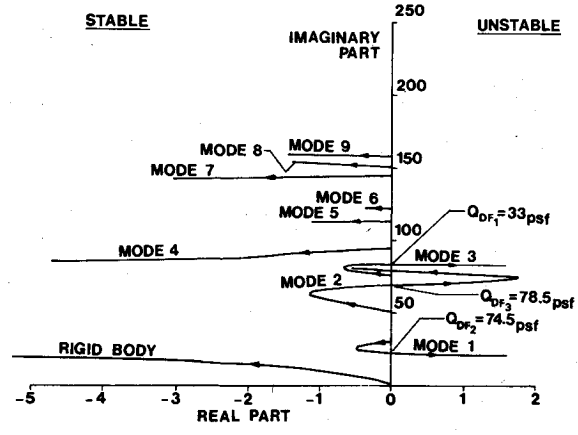


**Fig. 4 Open-loop root locus plot at $M=0.9$.**

for control law II to $Q_{DF}=89$ psf (with $g=0$ in both cases). The attempts to increase the values of this flutter branch beyond $Q_{DF}\approx90$ psf were not successful. This result is interesting since the relaxed energy approach does not ensure the suppression of flutter in all cases, due to the fact that it does not turn all the aerodynamic energy eigenvalue positive (in the case of the activated t.e. alone system). For a l.e.-t.e. system the suppression of flutter is ensured since all the aerodynamic energy eigenvalues assume positive values. Table 1 supplements the abovementioned results to include the effects of structural damping on the flutter speeds.

If we disregard the increase in flutter speed of each flutter branch and view the overall increase in flutter speed of the SST model, we arrive at the following conclusions: 1) the largest increase in flutter speed is for $g=0$, yielding an increase of 67%, whereas the smallest increase in flutter speed is for $g=0.03$, yielding an increase of 33%. 2) The variation of the overall flutter speed of the system with the dynamic pressure at which the optimization of the control parameters is performed is very small. This is illustrated in Fig. 7 where it can also be seen that the maximum flutter dynamic pressure is obtained when $Q_{DF}$ is equal to the value of the optimization $Q_D$ (that is around 90 psf). Finally, control law I was tested for flutter at $M=0.9$ yielding the value of $Q_{DF}=76$ psf for $g=0$ and $Q_{DF}=78$ psf for $g=0.03$ (see Fig. 8).

Figure 9 shows a comparison between the results obtained in the present work and those reported in Ref. 1. As can be seen, the closed-loop flutter speeds obtained herein are

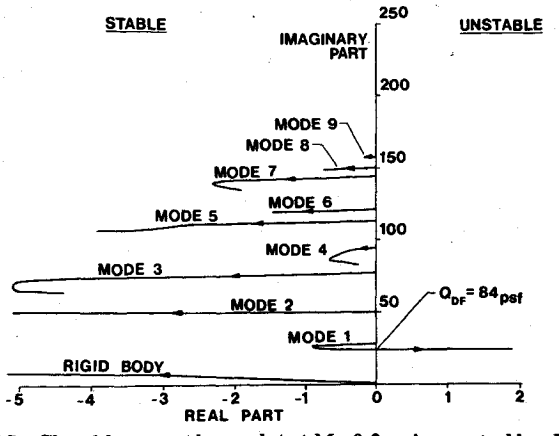


Fig. 5 Closed-loop root locus plot at $M=0.2$, using control law I.

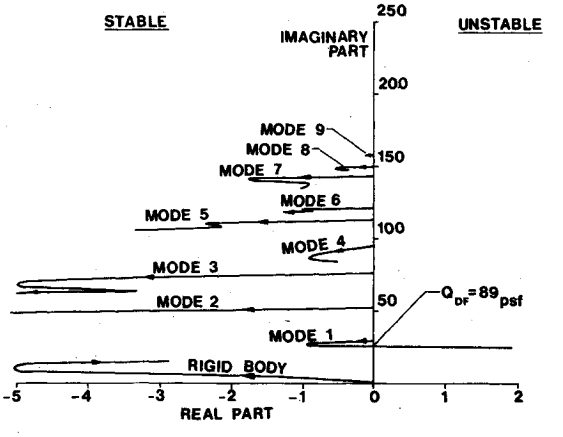


Fig. 6 Closed-loop root locus plot at $M=0.2$, using control law II.

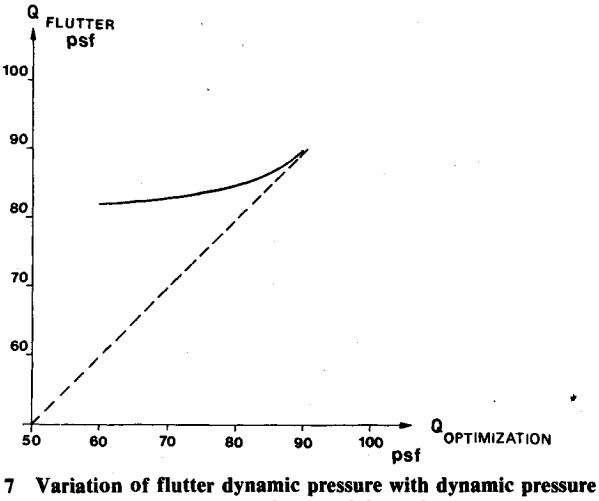


Fig. 7 Variation of flutter dynamic pressure with dynamic pressure at which optimization is performed at $M=0.2$ ($g=0$).

substantially more effective than those reported in Ref. 1 for the same SST flutter model with $g=0.03$ and $M=0.2$.

*Control Surface Activity*

The activity of the t.e. control (due to the different control laws) at the various flight dynamic pressures is shown in Figs. 10 and 11 for various values of $g$. It can be seen that control law II requires about 3.3 times as large rms control deflections as control law I, whereas rms control rates are larger by about 66% compared with control law I. Hence control law I appears to be better especially when considering that the difference between the overall flutter speeds due to those two

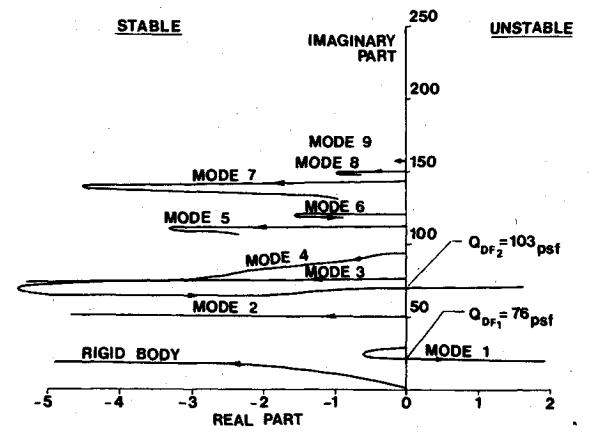


Fig. 8 Closed-loop root locus plot at $M=0.9$, using control law I.

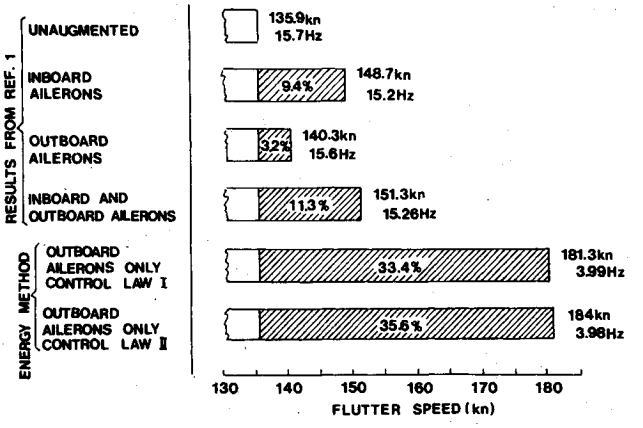


Fig. 9 Comparison between various results for the SST model at $M=0.2$.

control laws is small. Figure 12 shows that the control surface activity of control law I at $M=0.9$ is smaller than the activity at $M=0.2$

**Wing Root Bending Moment Alleviation**

The quantitative effect of the activated t.e. system on the rms wing root bending moment (b.m.) is meaningful only for flight speeds which are below the open loop flutter speeds. For speeds above the open-loop flutter speed the nonactivated rms wing root b.m. must clearly assume infinite values. Therefore, for flight speeds which lie between the open- and closed-loop flutter speeds the alleviation must therefore be infinite since the closed-loop system clearly yields finite rms values of b.m. The results to be presented herein will therefore relate to a range of dynamic pressures up to 32 psf which represents the open-loop value of $Q_{DF}$ for $g=0$ and $M=0.2$. No attempt will be made to change the above value of $g$ or the above value of $M$. Figure 13 shows the variation with flight dynamic pressure of the rms bending moment ratio, defined as the ratio between the closed-loop and open-loop rms b.m. [denoted as $(\text{b.m.})/(\text{b.m.})_0$] for the abovementioned two control laws. Figure 14 shows the variation with $Q_D$ of the ratio between the peak open- and closed-loop values of the b.m. as obtained from a PSD plot, an example of which is shown in Fig. 15 (with $Q_D=26$ psf using control law I). As can be seen, the alleviation in peak bending moments is much larger than the alleviation in rms b.m. at comparable values of $Q_D$. It is also interesting to note that control law II is more effective in reducing peak values of b.m. and relatively ineffective (that is, yields only minor improvements over the results obtained from control law I) in reducing rms b.m. values. Hence, the increase in the control activity associated with control law II, although ineffective for flutter suppression appears to be effective for peak b.m. alleviation.

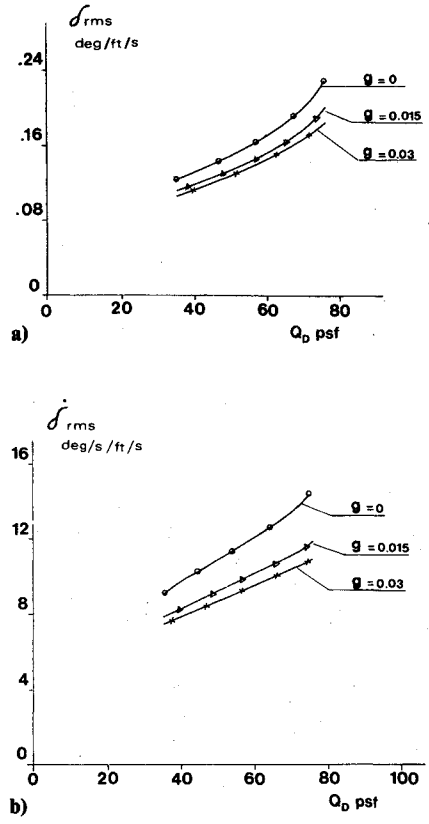


**Fig. 10 Variation of control surface activity with dynamic pressure (for various values of structural damping) at $M=0.2$, using control law I ($g=0$): a) control surface deflection, b) control surface rate.**

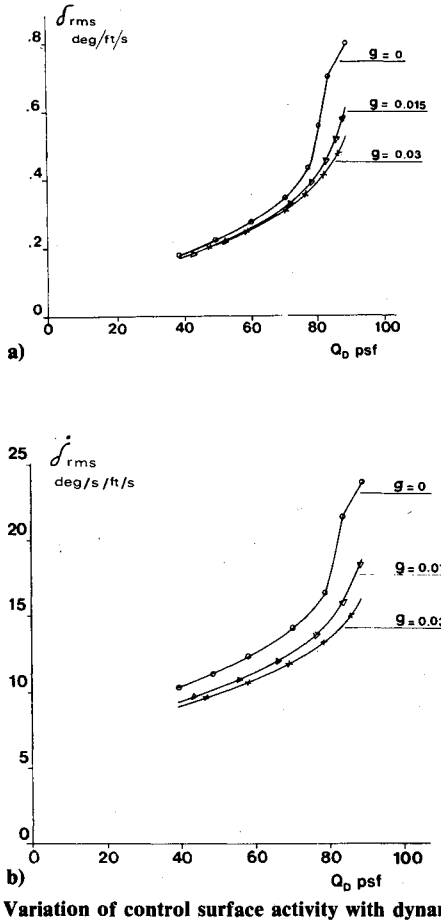


**Fig. 11 Variation of control surface activity with dynamic pressure (for various values of structural damping) at $M=0.2$, using control law II ($g=0$): a) control surface deflection, b) control surface rate.**

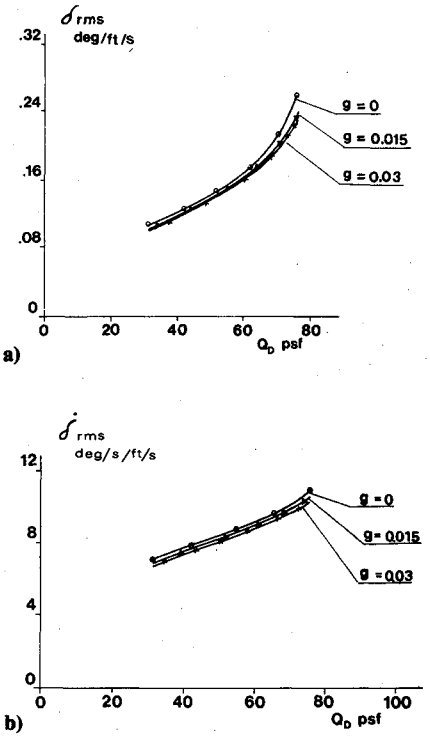


**Fig. 12 Variation of control surface activity with dynamic pressure (for various values of structural damping) at $M=0.9$, using control law II ($g=0$): a) control surface deflection, b) control surface rate.**

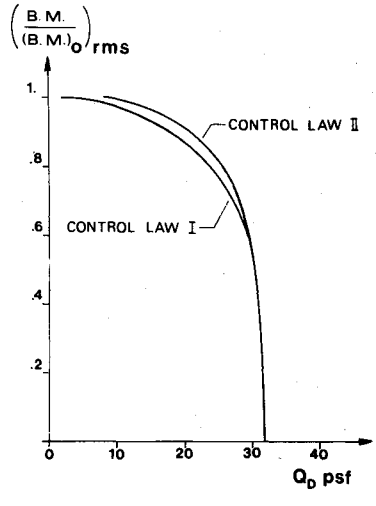


**Fig. 13 Variation of rms wing root bending moment ratio with flight dynamic pressure at $M=0.2$ ($g=0$).**

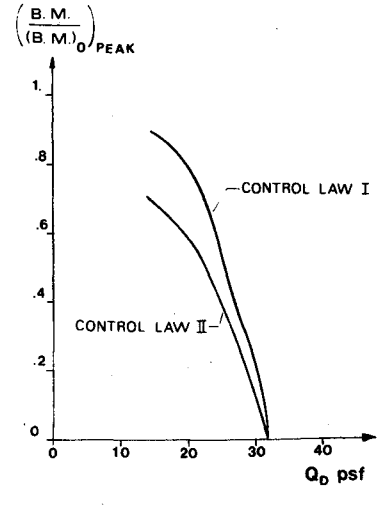


**Fig. 14 Variation of peak wing root bending moment ratio with flight dynamic pressure at $M=0.2$ ($g=0$).**

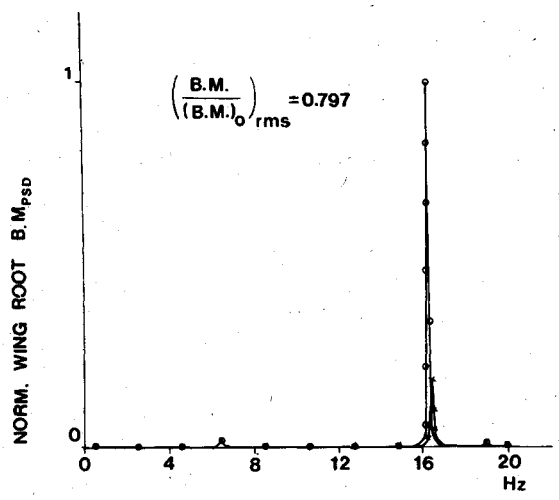


Fig. 15 PSD representation of normalized wing root bending moment at $M=0.2$ and $Q_D=26$ psf, using control law I.

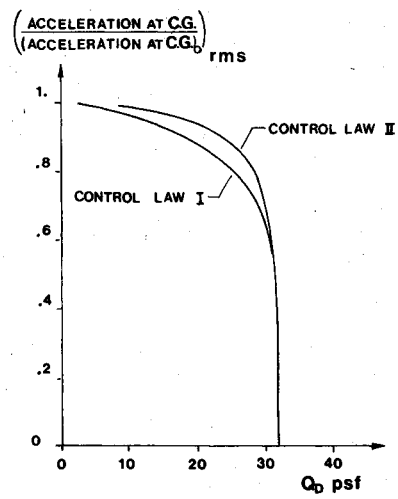


Fig. 16 Variation of rms acceleration ratio at c.g. with flight dynamic pressure at $M=0.2$ ($g=0$).

### Acceleration Alleviation

For reasons similar to those given in the case of the b.m. alleviation, the acceleration alleviation is relevant for flight speeds up to the open-loop flutter speed. Here again, only the case relating to $g=0$ and $M=0.2$ will be treated. Figure 16 shows the variation of the rms acceleration ratio (defined as the ratio between the closed-loop and open-loop rms accelerations) at the center of gravity (c.g.) of the SST model. Figure 17 shows the variation of the peak acceleration ratio at c.g. The results here are similar to those obtained for the b.m. ratio, that is, the activated systems are much more effective in reducing peak c.g. acceleration than in reducing rms accelerations at c.g. Similarly, control law II is relatively more effective in reducing peak c.g. accelerations than in reducing rms accelerations (compared with control law I).

The variation with $Q_D$ of the rms acceleration ratio for a point on the wing located at the midchord of the midspan section of the outboard control surface (to be referred to as the wing point) is shown in Fig. 18. The ratio between the peak accelerations at the above point with and without activation of the control surface is shown in Fig. 19 as a function of $Q_D$. As can be seen, the activated t.e. system is effective in reducing both the rms and the peak values of the accelerations at the above wing point. Here, control law II is substantially more effective than control law I in reducing both the peak acceleration ratio (similar to previously discussed cases) and the rms acceleration ratio (unlike previous cases where the difference was small).

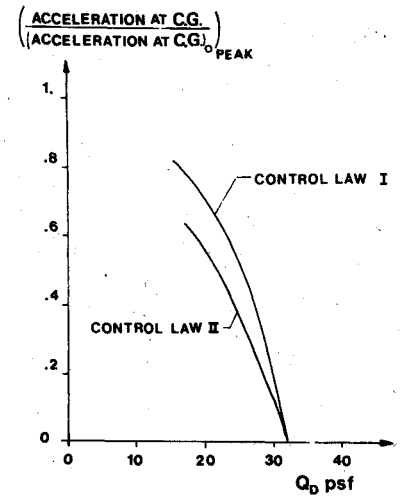


Fig. 17 Variation of peak acceleration ratio at c.g. with flight dynamic pressure at $M=0.2$ ($g=0$).

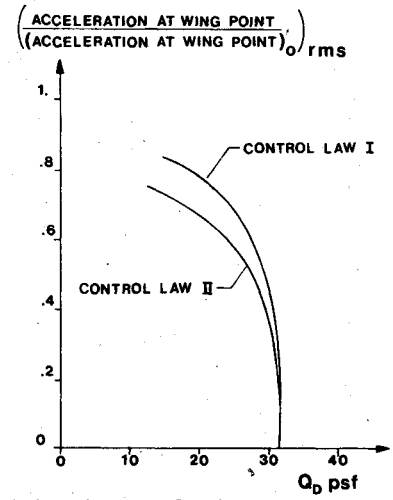


Fig. 18 Variation of rms acceleration ratio at wing point with flight dynamic pressure at $M=0.2$ ($g=0$).

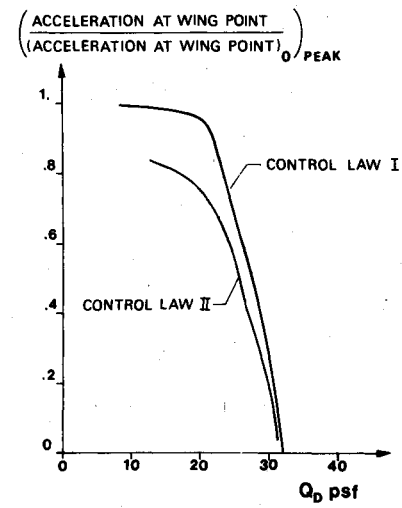


Fig. 19 Variation of peak acceleration ratio at wing point with flight dynamic pressure at $M=0.2$ ($g=0$).

## Conclusions

The application of the relaxed aerodynamic energy method coupled with the previously developed synthesis techniques yields effective flutter suppression systems when applied to the SST flutter model. The effectiveness of the control laws obtained herein substantially exceed the effectiveness of

similar systems designed by classical methods as reported in Phase II of the SST Technology Follow-on Program. The application treated in this work follows two successful applications relating to the BQM-34E/F drone aircraft (DAST Program) and to the VF-17 external store flutter suppression program, as mentioned earlier in this paper. The beneficial effects of the flutter suppression system on both gust alleviation and ride control problems are in agreement with a previous work involving combined l.e.-t.e. control systems based on the original formulation of the aerodynamic energy method.

Cases can be envisaged where the effectiveness of the t.e. control system, based on the relaxed energy method, will be of doubtful nature. Such a case was encountered in this work when trying to increase the flutter speed associated with the second flutter branch. It is however felt that when such cases do arise, an alternative location of the activated control surface might prove to overcome this difficulty. Alternatively, a combined l.e.-t.e. control system might be attempted. Finally, it might be worth noting that the control surface activity as obtained from the derived control laws in the present application is within present-day technology capability.

## Acknowledgments

The work reported herein is a part of a study supported by NASA through its Aeroelasticity Branch at the Langley Research Center (under Grant NSG 7373). The numerical data for the 2707-300 airplane was supplied by the Boeing Company.

## References

[1] Gregory, R.A., Ryneveld, A.D., and Imes, R.S., "SST Technology Follow-On Program-Phase II—A Low Speed Model Analysis and Demonstration of Active Control Systems for Rigid-Body and Flexible Mode Stability," Boeing Commercial Airplane Company, Seattle, Wash. Rept No. FAA-SS-73-18, June 1974.

[2] Nissim, E., "Recent Advances in Aerodynamic Energy Concept for Flutter Suppression and Gust Alleviation Using Active Controls," NASA TN D-8519, Sept. 1977.

[3] Nissim, E. and Abel, I., "Development and Application of an Optimization Procedure for Flutter Suppression using the Aerodynamic Energy Concept," NASA TP1137, FEb. 1978.

[4] Nissim, E. "Comparative study Between two Different Active Flutter Suppression Systems," Journal of Aircraft, Vol. 15, Dec. 1978, pp. 843-848.

[5] Nissim, E. and Lottati, I., "Active External Store Flutter Suppression in the YF-17 Flutter Model," *Journal of Guidance and Control,* Vol. 2, Sept.-Oct. 1979, pp. 395-401.

[6] Nissim, E., Caspi, A., and Lottati, I., "Application of the Aerodynamic Energy Concept to Flutter Suppression and Gust Alleviation by Use of Active Controls," NASA TN D-8212, June 1976.

[7] Sevart, F.D., "Development of Active Flutter Suppression Wind Tunnel Testing Technology," AFFDL-TR-74-126, 1975.

[8] Pratt, K.G., "Response of Flexible Airplanes to Atmospheric Turbulence. Performance and Dynamics of Aerospace Vehicles," NASA SP-258, March 1971, pp. 439-503.

[9] Nissim, E., "Flutter Suppression Using Active Controls Based on the Concept of Aerodynamic Energy," NASA TN D-6199, March 1971.